

Communication

Fiber-Fed 3D Printing of Germanate Glass Optics

Zhihan Hong ^{1,*}, Tao Luo ², Shibin Jiang ² and Rongguang Liang ^{1,*}¹ Wyant College of Optical Sciences, The University of Arizona, 1630 E University Blvd, Tucson, AZ 85721, USA² Advalue Photonics Inc., 2700 E Bilby Rd., Tucson, AZ 85706, USA

* Correspondence: zhihanhong@arizona.edu (Z.H.); rliang@optics.arizona.edu (R.L.)

Abstract: In recent years, 3D printing glass optics has gained massive attention in industry and academia since glass could be an ideal material to make optical elements, including the lens. However, the limitation of materials and printing methods has prevented 3D printing glass optics progress. Therefore, we have developed a novel printing strategy for germanate glass printing instead of pure silica. Moreover, compared with traditional multi-component quartz glass, germanate glass has unmatched advantages for its mid-infrared (MIR) transparency and outstanding visible light imaging performance. Furthermore, compared with non-oxide glass (fluoride glass and chalcogenide glass), germanate glass has much better mechanical, physical, and chemical properties and a high refractive index. Germanate glass has been widely applied in remote sensing, ranging, environmental detection, and biomedical detection. However, it is difficult to shape, cast, polish, and grind for optical and photonics applications such as imaging optics and laser-collimation optics. These drawbacks have made germanate glass inaccessible to complex optical elements and greatly increased their cost. In this report, we use germanate glass fibers with a diameter of 125 μm based on fiber-fed laser heating technology to fabricate an mm-size optical application. In this paper, we combine the fiber-fed laser heating technology with an optimized temperature control process to manufacture high-precision optical elements. Germanate glass optics can be printed with excellent visible light and IR transparency and a smooth surface with roughness under 4 nm. By optimizing the layer-by-layer 3D printing process and the thermal feedback in the printing process, we avoid cracks and minimize surface deformation. This work shows the possibility of the mm-size glass optical elements 3D printing and widens its application for IR optics.

Keywords: 3D printing; glass; infrared; germanate; laser; lens; imaging; biomedical; collimator; fiber-fed; temperature control



Citation: Hong, Z.; Luo, T.; Jiang, S.; Liang, R. Fiber-Fed 3D Printing of Germanate Glass Optics. *Photonics* **2023**, *10*, 378. <https://doi.org/10.3390/photonics10040378>

Received: 12 February 2023

Revised: 24 March 2023

Accepted: 27 March 2023

Published: 29 March 2023



Copyright: © 2023 by the authors. Licensee MDPI, Basel, Switzerland. This article is an open access article distributed under the terms and conditions of the Creative Commons Attribution (CC BY) license (<https://creativecommons.org/licenses/by/4.0/>).

1. Introduction

Nowadays, 3D printing technology has started to release its potential in manufacturing and more modern functionalities such as biomedical [1], automotive and aerospace [2], and construction [3] are being developed. Three-dimensional printing optics has become a possible solution for complex geometrical optics. Polymer-optics 3D printing has been substantially researched and developed [4–11]. However, 3D printing glass optics still faces challenges from manufacturing accuracy, shrinkage, and material limitation [12–25]. The most common approaches for glass 3D printing, including direct printing, transparent inorganic glass optics with laser sintering, fused filament deposition, direct ink writing (DIW), stereolithography (STL), projection microstereolithography (P μ SL), or two-photon stereolithography (TPSL), have generally not achieved the quality required for optical applications [4–6,8,9,13,15–18,25–29]. These approaches have been limited by shrinkage, the burning out of organic components and high-temperature sintering, defects (bubbles, hidden layers, etc.), and material limitations. These have prevented inorganic glass from becoming a reliable material for modern optic printing. Although the solvent-free, silica precursor, and two-photon polymerization process have highly decreased the shrinkage and deformation through pyrolysis to avoid the sintering process [13,25,27]. The challenge

of printing glass optics into mm-size remains due to the time consumption from its direct laser writing (DLW) process, such as two-photon polymerization (TPP) or two-step polymerization (TSP) [11,30–33].

In addition, it is extremely tough to develop different glass materials to fit different optical properties such as the refractive index, abbe number, and transmittance. Fused glass filament deposition of inorganic glass fiber also suffers from low print resolution due to the size of the filament, and the CO₂ laser-induced temperature variation highly increases the difficulties in controlling the layer thickness. Meanwhile, the glass fiber feeding process and translation stage movement may suffer from changes in the glass viscosity, which can stimulate adverse effects in each layer [15–17].

In this paper, we resolve the limitation of material by using germanate glass instead of silica and manufacture an accurate spherical lens with a diameter from millimeter size to centimeter size and prove the possibility of printing a complex aspherical lens. We develop a germanate glass fiber-fed laser-melting method with the temperature keeping and feedback system (GFLFS) to control a stable layer thickness for the input germanate glass fiber (GGF). Printing is carried out by laser melting and feeding germanium glass fiber on the germanate glass slide with a CW CO₂ laser. We demonstrate that the germanate glass lens can be printed accurately with a peak to valley <600 nm and a surface roughness lower than 4 nm. Furthermore, the printed lens can collimate 632.8 nm and 1.7 μm laser beams. Simultaneously, the printed lens is used to make a microscopy system and proves the potential for biomedical imaging. Germanate glass, a popular near infrared glass fiber material, is also a great choice for visible light and IR imaging optics, which has a large refractive index, $n = 1.6555$ at 589 nm wavelength and $n = 1.6399$ at 1 μm wavelength, showing that it is suitable for visible, NIR, SWIR, and MWIR applications [34–43].

2. Materials and Methods

Figure 1a is the layout of the GFLFS platform. A CW CO₂ laser ($\lambda = 10.6\mu\text{m}$) melts the fed GGF and prints the structure on the germanate glass substrate. Figure 1b shows that the GGF feeding process, and the prepared GGF feeding speed can be highly controlled through the aluminum feeding tube. The substrate is fixed on the temperature control system with a temperature feedback circuit in Figure 1a. Figure 1c,d show the top view and the side view of the schematic diagram set on the insulation system in Figure 1a. Instead of using a simple heating plate, we built a ceramic insulation material bulk to improve the temperature control accuracy and decrease the thermal expansion difference between the printed lens and the substrate. The substrate is pre-manufactured with the same diameter as the designed lens. We also can cut the substrate to fit the lens diameter if we print more than one lens per substrate.

Figure 2a shows the glass lens manufacturing process. As Figure 2c shows, the temperature control strategy mainly divides into 4 parts: pre-heating, printing, stress releasing, and cooling. The substrate is pre-heated to T_g ($\sim 450^\circ\text{C}$) in ~ 30 min, and then we print the lens structure layer-by-layer (Figure 2b). After the lens printing, to alleviate the residual inner stresses and to avoid cracking (Figure 2f), the temperature is increased to $\sim 500^\circ\text{C}$ by $10^\circ\text{C}/\text{min}$ for 30 min for a 5 mm-diameter lens and slowly decreased to 30°C below T_g ($2^\circ\text{C}/\text{min}$) for 30 min. Finally, the temperature is cooled down to room temperature by $2^\circ\text{C}/\text{min}$.

It should be noted that the time of the printing process is determined by the lens size and printing resolution. We manufacture the lenses with GGF with different diameters (125 μm and 150 μm). Figure 2d shows the printing process with the fixed parameters, 0.15 mm/s feeding speed and 0.15 mm/s translation moving speed. The laser focal spot diameter is around 0.8 mm. We use an external voltage board to switch and control the laser power by changing the voltage, amplitude, and frequency. The manufacturing laser power range has been optimized to set the manufacturing window from 16 W to 41 W to avoid cracks in the printing process. Figure 2d shows an example of the optimized printed glass curve performance. The layer thickness and diameter were analyzed based on the

default parameters. The feeding volume (FV) per second can be simplified as a cylinder. In the printing process, FV depends on the feeding speed (FS) and the diameter of the glass fiber (D).

$$FV = \pi(D^2/4) \times FS(s^{-1})$$

Although FV is stable for constant fiber diameter and feeding speed, the different input power will change the aspect ratio (AR) of its cross-section.

$$AR = height / diameter$$

Figure 2e shows the relationship between the height and diameter of the printed single line for different laser powers. The height of the printed line decreased for different laser powers, and the diameter increased simultaneously, meaning that the axis printing resolution can be controlled by the laser power or the diameter of the fed glass fiber.

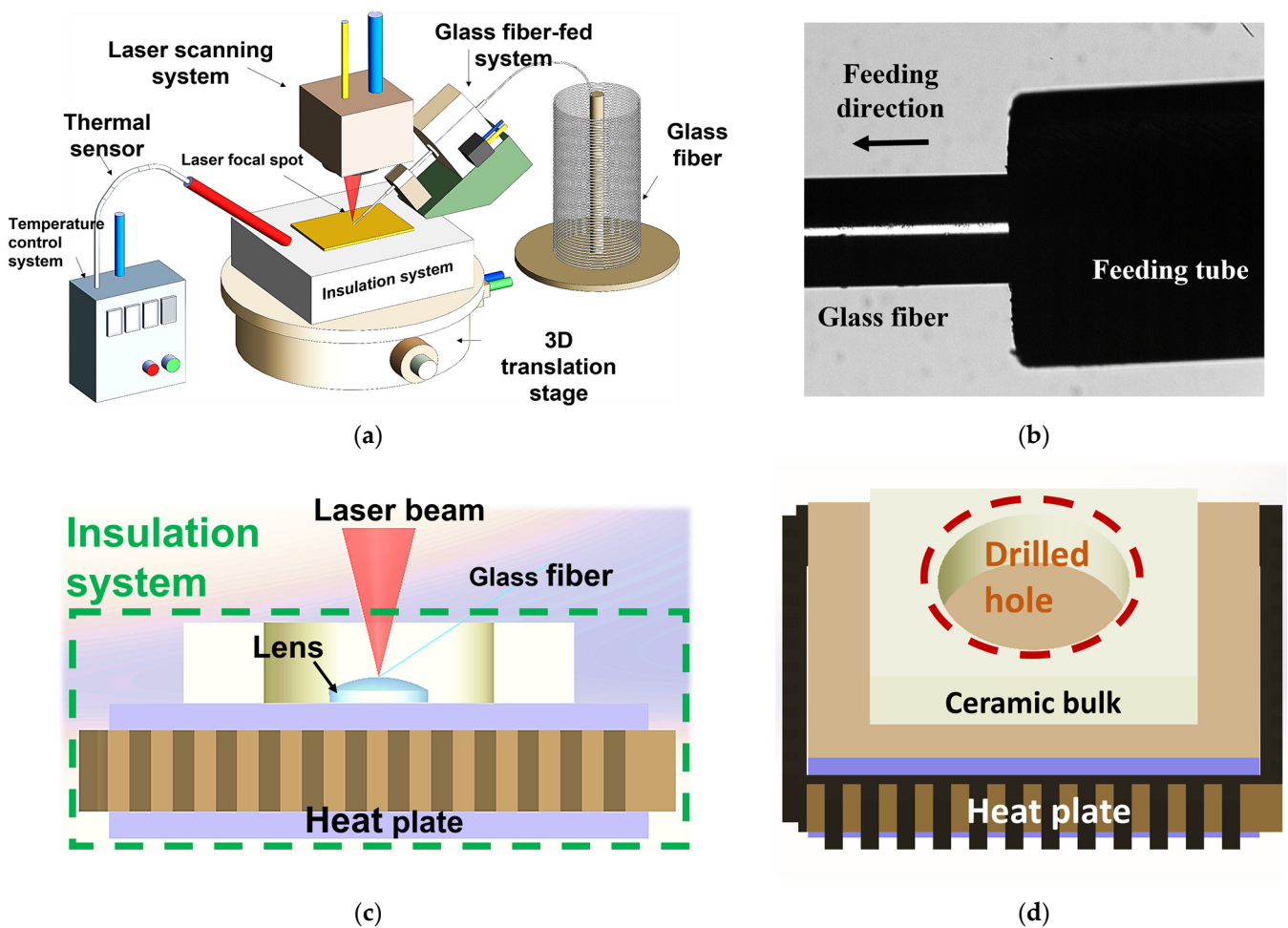


Figure 1. Printing system and printing process. (a) Schematic diagram of the 3D printing system including fiber-fed system, laser-melting system and temperature control system; (b) The fiber-feeding process including the aluminum tube and GGF; (c,d) The top view and side view of the schematic diagram of self-build ceramic insulation material bulk.

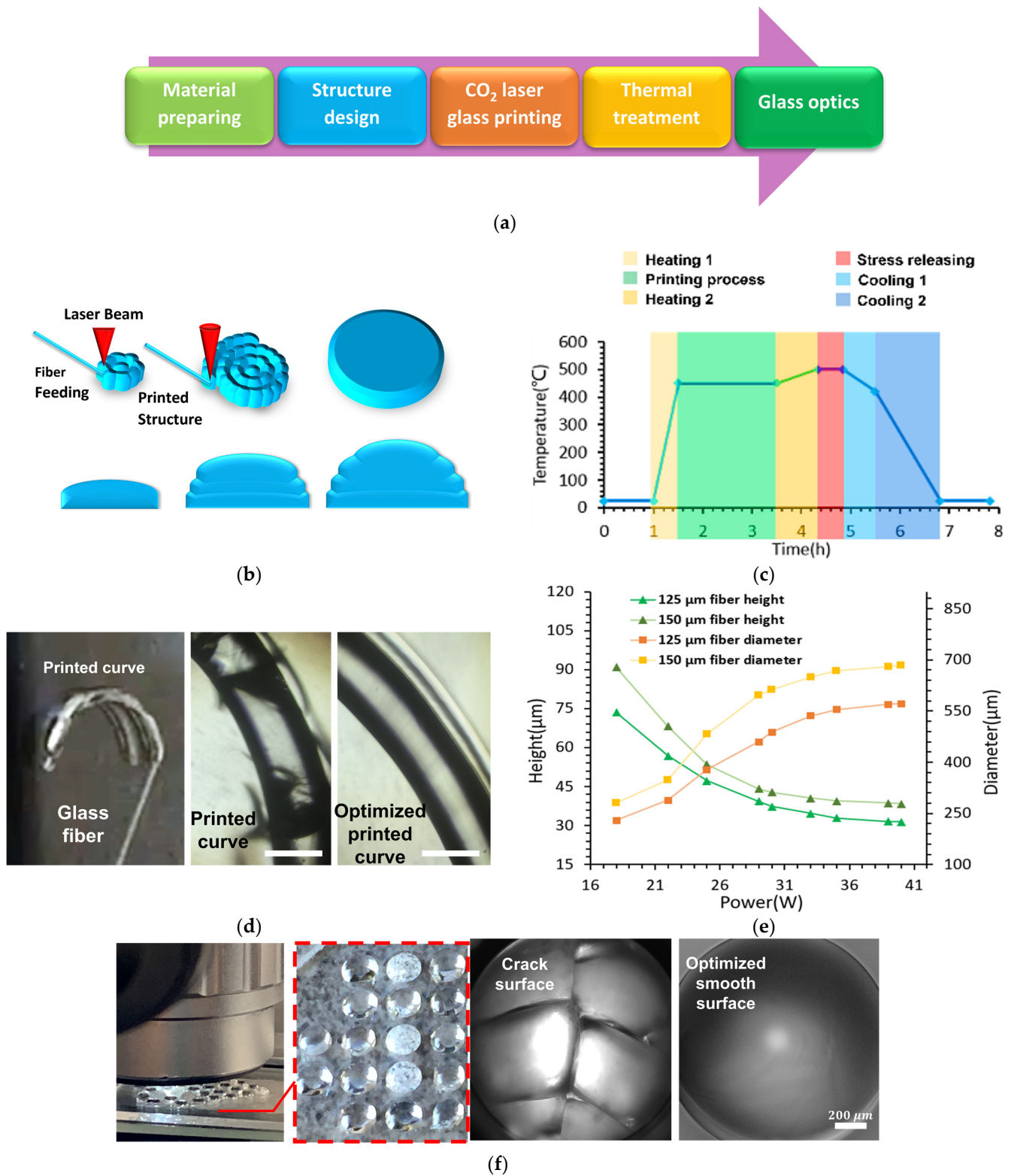


Figure 2. (a) The diagram of glass lens fabrication process; (b) The diagram of layer-by-layer printing process; (c) The strategy of temperature control during the manufacturing process; (d) The example for line printing and the optimized smooth printed glass line (scale bar: 100 μm); (e) The printing resolution with a staple feeding and stage moving speed at 0.15 mm/s; (f) The crack surface and smooth surface comparison.

3. Fabrication Results

Additionally, the temperature control time is positively proportional to the diameter and the sag height of the lenses. For example, it takes around 35 min for the 3 mm sag and 5 mm-diameter lens. Figure 3a shows a 5 mm-diameter plano-convex spherical lens printing process and the clear lens after thermal treatment. Figure 3c shows two manufactured plano-convex germanate glass lenses with the same parameters, where the lenses are 3.75 mm in diameter and 5.15 mm radius of curvature. The surface profile was detected by a white-light interferometer (Figure 3d). Surface deviation from the ideal lens surface in the central region was less than ± 300 nm (Figure 3e). RMS surface roughness (Sq) was less than 1 nm (Figure 3f). The fabricating method proves reliability and allows the possibility for excellent surface performance manufacturing.

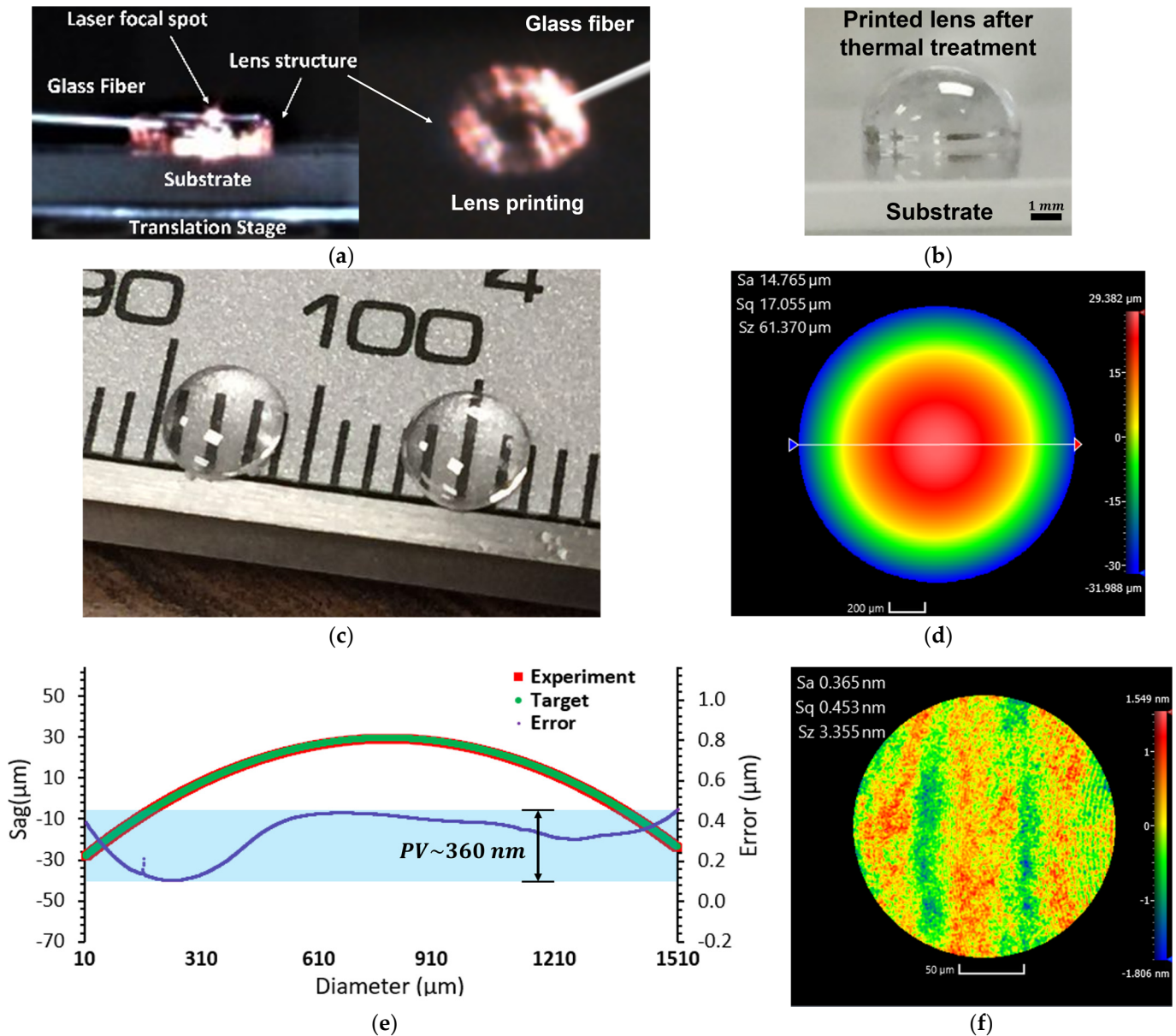


Figure 3. (a) The lens with 5 mm-diameter printing process; (b) The manufactured plano-convex lens after fully stress releasing; (c) The image of two printed glass lenses with same surface curvature, thickness and diameter; (d) The surface profile of the printed lens in (c); (e) Surface deviation of the printed lens in (c); (f) The surface roughness of the printed lens in (c). ((d,f) detected by Zygo Newview 8300 optical white light interferometer).

4. Experiment Results

Considering the excellent transmittance in visible and infrared bandwidth of germanate glass, the transmission measurement from 1.5 μm to 5.5 μm is shown in Figure 4b. The germanate glass thick plate (3.6 mm thickness) shows a high transmission, nearly 90% in the range of 1.5 μm to 3.5 μm , and transmission $>70\%$ at 4 μm . Then, we developed the laser collimator, which has become an available application to evaluate its performance. Figure 4a shows the designed laser-collimating system, including the multimode fiber mount, lens mount, and adjustable part. The assembled printed germanate glass lens can adjust the distance between the lens and the fiber output end. It can flexibly control the diverse angle of the collimated IR (wavelength $\sim 1.7 \mu\text{m}$) laser beam. We can clearly observe a collimated circle-like beam pattern on the IR card. Figure 4c shows the designed single-mode fiber (SMF) for a 632.8 nm laser. Multimode fiber and SMF mount were manufactured by the commercial 3D printer using plastic material. The collimated 632.8 nm laser beam has been appropriately demonstrated to propagate through the interference pattern in Figure 4d.

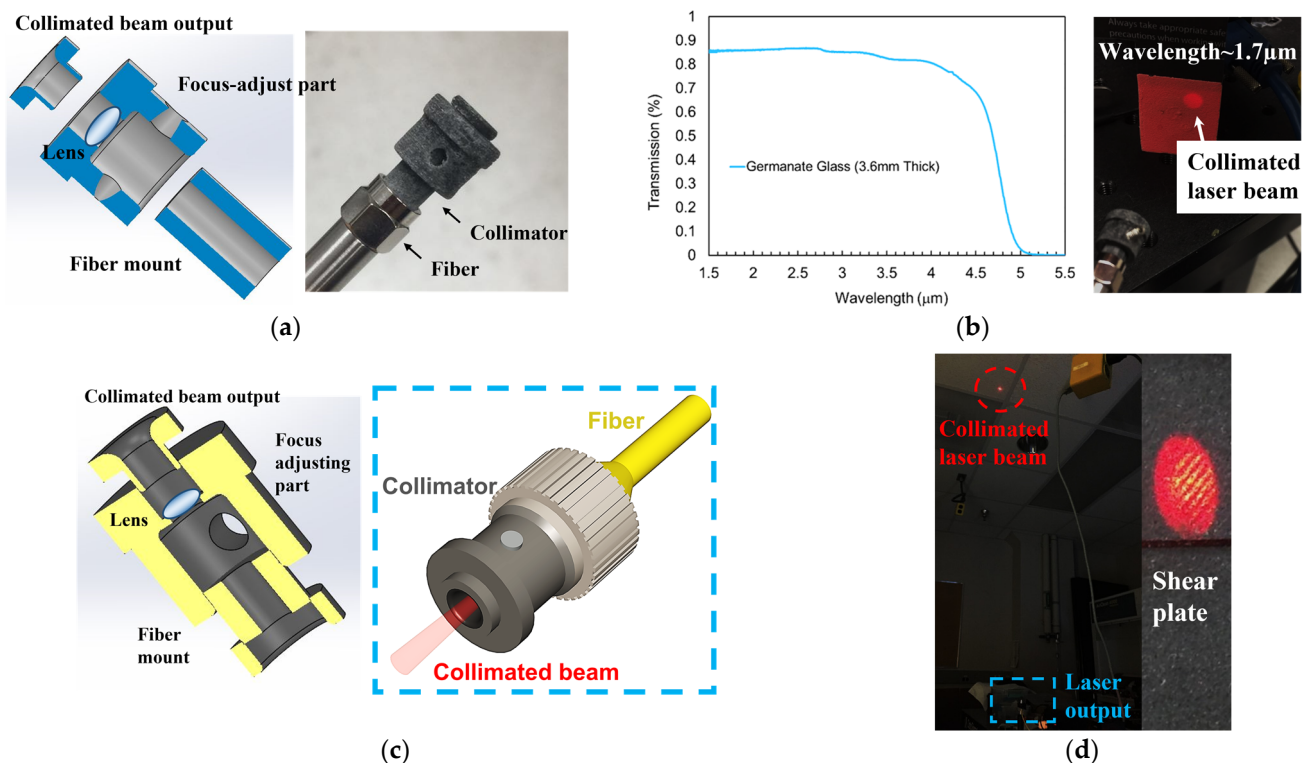


Figure 4. (a) Schematic diagram of the designed mount for laser collimator including multimode fiber mount, lens mount and the side-view of the manufactured laser collimator and the laser fiber; (b) The collimated 1710 nm wavelength laser beam performance on the IR card; (c) The design of the collimator structure for single-mode fiber and the single-mode fiber with the mounted collimator; (d) The beam spot after collimating the fabricated collimator and the inference by the shear plate.

Therefore, the laser collimator can also be utilized for IR and visible wavelength laser beams. The detected laser divergence dimension of 632.8 nm and 1.7 μm laser beams, as shown in Figure 5a,b, offers an available specification for industrial possibilities.

Further analyzing the glass 3D printing performance of the lens, we designed a microscope system for a cell phone camera. Figure 6a shows the experiment setup, and we set the optical system in front of the cell phone camera. Figure 6b shows the image of the USAF 1951 resolution target by the printed glass objective. The 6th term from the 6th group (the highest resolution of the target) of the target has been captured clearly, at 114 lp/mm.

The system can be used to test the bio-sample. Figure 6c shows the image of onion pulp cells. The outline of each cell is observed.

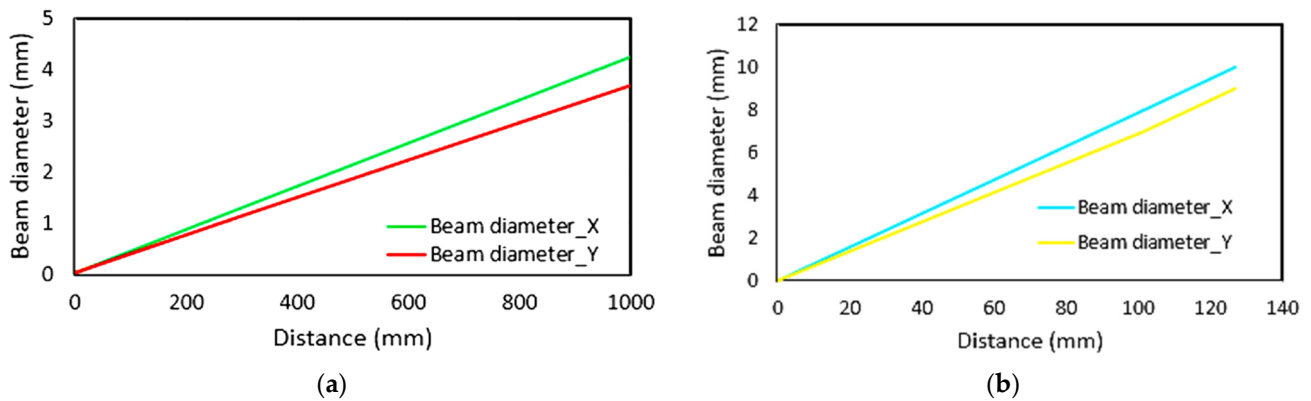


Figure 5. (a) The divergence dimension performance of 632.8 nm laser beam; (b) The divergence dimension performance of 1.7 μm laser beam.

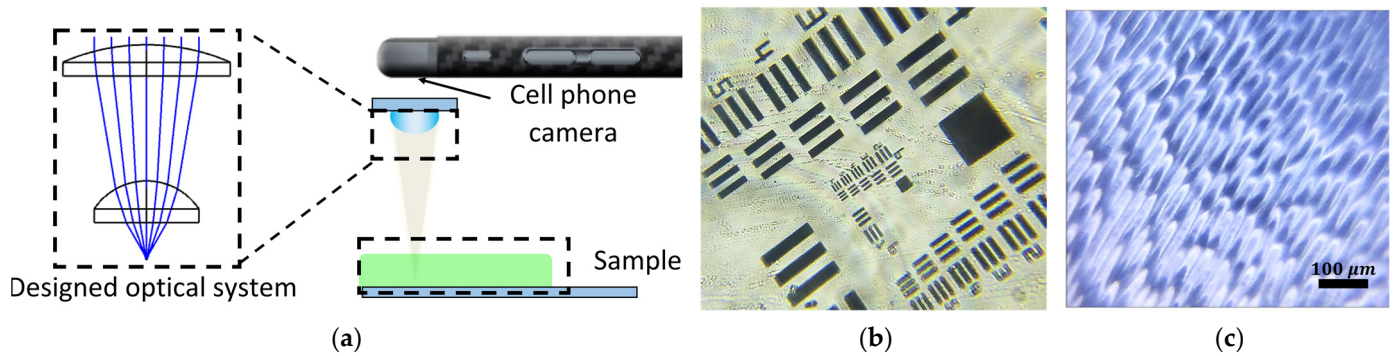


Figure 6. (a) The designed microscopy layout and the diagram of the experiment set up; (b) The image of 1951 USAF resolution target. (c) The image of onion pulp cells.

Furthermore, we printed the aspherical donut-shape-like lens in Figure 7b. The diameter of the lens is ~4 mm, and the thickness is ~2 mm. From its center to the edge-side of the printed lens, the bent image explains the capability of its radius of curvature distribution. As the side view of the designed printing strategy shows in Figure 7a, the a, b, and c curves are convex, concave, and convex. Like spherical lens printing, the printing resolution is also controlled by layer thickness. The printed non-spherical lens further demonstrates the manufacturing flexibility of our proposed method.

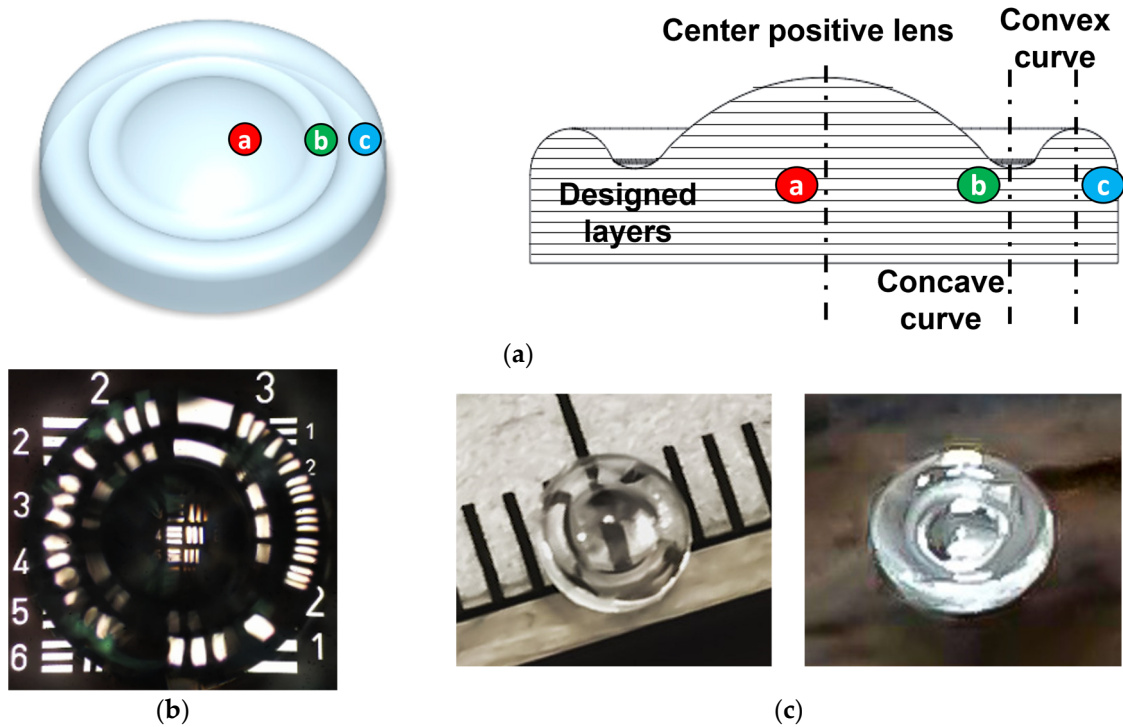


Figure 7. (a) The design of the donut-shape lens and layer-by-layer printing strategy; (b) donut-shape lens showing ray bending; (c) The images of the donut-shape lens on the caliper and desk.

5. Conclusions and Discussion

We developed the laser-heat germanate glass optics 3D printing method using the optimized temperature feedback circuit fiber-fed system. The proposed method was not only used for printing the single spherical lens but for the multi-lens microscopy imaging system build and the continuous surface manufacturing. The surface roughness is lower than 1 nm, and the surface deviation peak-to-valley (PV) value is lower than 600 nm (± 300 nm), which meets the commercial standard for imaging optics and pioneers the accurate millimeter size glass imaging optics printing. Compared to the 3D-printed glass optics through the methods such as two-photon polymerization, direct laser writing, direct ink writing, glass deposition, and glass filament feeding, we upgraded the available glass optics printing method for “Macro” optical elements, including laser collimator and microscope without the shrinkage and cracks. Moreover, we have created new potential for germanate glass and its excellent properties, such as thermal stability, mechanical properties, chemical resistance, and imaging performance in visible light, NIR, and MIR regions. Moreover, instead of pure silica, we utilized complex doped glass to break through the material limitation by its different refractive index and transmittance. We believe that the reported research not only paves the way for low-cost fabrication of complex IR glass optical systems for imaging applications but also develops the heating strategy for glass additive manufacturing, including preheating, the printing process, and inner stress-releasing corresponding to the glass transition temperature (T_g).

The proposed printing method and laser heating process for printing precise optical elements still face major limitations in the complex optical imaging system. Double-let lens manufacturing needs an accurate optical axis alignment for up-surface and down-surface. Additionally, the 3D printing process will print millimeter-size components and centimeter-size optics for more imaging optics with larger apertures, such as camera lenses, especially the infrared (IR) camera lens, significantly reducing the cost. Figure 8a,b demonstrate a manufactured plano-convex germanate visible-IR lens with around 20 mm diameter and more positive lenses with different sag heights and diameters. It should be mentioned that the micro-bubbles mainly cause defects inside the lens during the fiber-feeding process,

which can be highly decreased by optimizing the temperature control and feeding stability. The OCT system will detect the uniformity of the refractive index inside the lens.

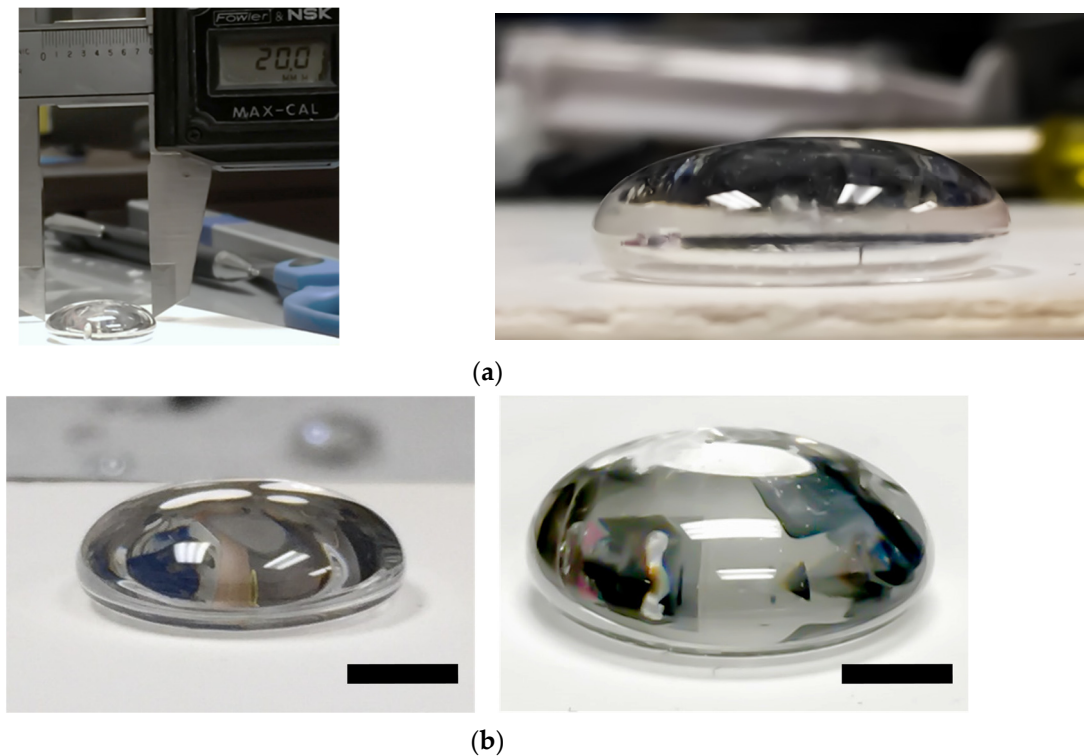


Figure 8. (a) The manufactured germanate glass lens with (20 ± 0.01) mm diameter; (b) The manufactured spherical lenses. (Scale bar: 5 mm).

With outstanding properties in resolution, dimension, and cost, we expect that the GFLFS system will have a variety of applications in astronomy, remote sensing, surveillance, biotechnology, medical diagnosis, agriculture, pharmaceuticals, food analysis, oil and gas detection, machine vision, etc., from visible to IR.

Author Contributions: Conceptualization, Z.H., T.L., S.J. and R.L.; methodology, Z.H., T.L.; software, Z.H. and S.J.; validation, Z.H., S.J. and R.L.; formal analysis, Z.H.; investigation, Z.H., S.J. and R.L.; resources, S.J., T.L. and R.L.; data curation, Z.H.; writing—original draft preparation, Z.H.; writing—review and editing, all authors; visualization, Z.H.; supervision, all authors.; project administration, S.J.; funding acquisition, S.J. All authors have read and agreed to the published version of the manuscript.

Funding: This research was partially supported by USAF/AFMC, grant number AFRL-2023-0530.

Institutional Review Board Statement: Not applicable.

Informed Consent Statement: Not applicable.

Data Availability Statement: Not applicable.

Conflicts of Interest: The authors declare no conflict of interest.

References

1. Dey, M.; Ozbolat, I.T. 3D bioprinting of cells, tissues and organs. *Sci. Rep.* **2020**, *10*, 14023. [[CrossRef](#)] [[PubMed](#)]
2. Duda, T.; Raghavan, L.V. 3D Metal Printing Technology. *IFAC-Pap.* **2016**, *49*, 103–110. [[CrossRef](#)]
3. Hager, I.; Golonka, A.; Putanowicz, R. 3D Printing of Buildings and Building Components as the Future of Sustainable Construction? *Procedia Eng.* **2016**, *151*, 292–299. [[CrossRef](#)]
4. Kang, W.; Hong, Z.; Liang, R. 3D printing optics with hybrid material. *Appl. Opt.* **2021**, *60*, 1809–1813. [[CrossRef](#)] [[PubMed](#)]
5. Liang, R.; Hong, Z. Laser-Assisted Additive Manufacture of Optics Using Thermally Curable Materials. U.S. Patent Application No. 16/484,310, 30 January 2020.

6. Li, Z.; Hong, Z.; Xiao, Y.; Hao, Q.; Liang, R. Thermal effects in single-point curing process for pulsed infrared laser-assisted 3D printing of optics. *3D Print. Addit. Manuf.* **2020**, *7*, 151–161. [[CrossRef](#)]
7. Assefa, B.G.; Pekkarinen, M.; Partanen, H.; Biskop, J.; Turunen, J.; Saarinen, J. Imaging-quality 3D-printed centimeter-scale lens. *Opt. Express* **2019**, *27*, 12630–12637. [[CrossRef](#)]
8. Chen, X.; Liu, W.; Dong, B.; Lee, J.; Ware, H.O.T.; Zhang, H.F.; Sun, C. High-speed 3D printing of millimeter-size customized aspheric imaging lenses with sub 7 nm surface roughness. *Adv. Mater.* **2018**, *30*, 1705683. [[CrossRef](#)]
9. Hong, Z.; Liang, R. IR-laser assisted additive freeform optics manufacturing. *Sci. Rep.* **2017**, *7*, 1–7. [[CrossRef](#)]
10. Takada, K.; Sun, H.-B.; Kawata, S. Improved spatial resolution and surface roughness in photopolymerization-based laser nanowriting. *Appl. Phys. Lett.* **2005**, *86*, 071122. [[CrossRef](#)]
11. Cumpston, B.H.; Ananthavel, S.P.; Barlow, S.; Dyer, D.L.; Ehrlich, J.E.; Erskine, L.L.; Heikal, A.A.; Kuebler, S.M.; Lee, I.Y.S.; McCord-Maughon, D.; et al. Two-photon polymerization initiators for three-dimensional optical data storage and microfabrication. *Nature* **1999**, *398*, 51–54. [[CrossRef](#)]
12. Mader, M.; Schlatter, O.; Heck, B.; Warmbold, A.; Dorn, A.; Zappe, H.; Risch, P.; Helmer, D.; Kotz, F.; Rapp, B.E. High-throughput injection molding of transparent fused silica glass. *Science* **2021**, *372*, 182–186. [[CrossRef](#)]
13. Hong, Z.; Ye, P.; Loy, D.A.; Liang, R. Three-dimensional printing of glass micro-optics. *Optica* **2021**, *8*, 904–910. [[CrossRef](#)]
14. Datsiou, K.C.; Saleh, E.; Spirrett, F.; Goodridge, R.; Ashcroft, I.; Eustice, D. Additive manufacturing of glass with laser powder bed fusion. *J. Am. Ceram. Soc.* **2019**, *102*, 4410–4414. [[CrossRef](#)]
15. Hostetler, J.M.; Johnson, J.E.; Goldstein, J.T.; Bristow, D.A.; Landers, R.G.; Kinzel, E.C. Fiber-Fed Printing of Free-Form Free-Standing Glass Structures. In Proceedings of the 29th Annual International Solid Freeform Fabrication Symposium, University of Texas at Austin, Austin, TX, USA, 13–15 August 2018; pp. 994–1002.
16. Nguyen, D.T.; Meyers, C.; Yee, T.D.; Dudukovic, N.A.; Destino, J.F.; Zhu, C.; Duoss, E.B.; Baumann, T.F.; Suratwala, T.; Smay, J.E. 3D-printed transparent glass. *Adv. Mater.* **2017**, *29*, 1701181. [[CrossRef](#)]
17. Luo, J.; Gilbert, L.J.; Qu, C.; Landers, R.G.; Bristow, D.A.; Kinzel, E.C. Additive manufacturing of transparent soda-lime glass using a filament-fed process. *J. Manuf. Sci. Eng.* **2017**, *139*, 061006. [[CrossRef](#)]
18. Kotz, F.; Arnold, K.; Bauer, W.; Schild, D.; Keller, N.; Sachsenheimer, K.; Nargang, T.M.; Richter, C.; Helmer, D.; Rapp, B.E. Three-dimensional printing of transparent fused silica glass. *Nature* **2017**, *544*, 337–339. [[CrossRef](#)]
19. Luo, J.; Gilbert, L.J.; Bristow, D.A.; Landers, R.G.; Goldstein, J.T.; Urbas, A.M.; Kinzel, E.C. Additive manufacturing of glass for optical applications. In *Laser 3D Manufacturing III*; SPIE: Bellingham, WA, USA, 2016; pp. 123–131.
20. Klein, J.; Stern, M.; Franchin, G.; Kayser, M.; Inamura, C.; Dave, S.; Weaver, J.C.; Houk, P.; Colombo, P.; Yang, M. Additive manufacturing of optically transparent glass. *3D Print. Addit. Manuf.* **2015**, *2*, 92–105. [[CrossRef](#)]
21. Fateri, M.; Gebhardt, A. Selective laser melting of soda-lime glass powder. *Int. J. Appl. Ceram. Technol.* **2015**, *12*, 53–61. [[CrossRef](#)]
22. Luo, J.; Pan, H.; Kinzel, E.C. Additive manufacturing of glass. *J. Manuf. Sci. Eng.* **2014**, *136*, 061024. [[CrossRef](#)]
23. Khmyrov, R.; Grigoriev, S.; Okunkova, A.; Gusarov, A. On the possibility of selective laser melting of quartz glass. *Phys. Procedia* **2014**, *56*, 345–356. [[CrossRef](#)]
24. Marchelli, G.; Prabhakar, R.; Storti, D.; Ganter, M. The guide to glass 3D printing: Developments, methods, diagnostics and results. *Rapid Prototyp. J.* **2011**, *17*, 187–194. [[CrossRef](#)]
25. Hong, Z.; Ye, P.; Loy, D.A.; Liang, R. High-Precision Printing of Complex Glass Imaging Optics with Precondensed Liquid Silica Resin. *Adv. Sci.* **2022**, *9*, 2105595. [[CrossRef](#)] [[PubMed](#)]
26. Xiao, Y.; Hong, Z.; Zhao, G.C.H.; Liang, R.; Lucas, P.; Hao, Q. Thermal studies of three-dimensional printing using pulsed laser heating. *ES Mater. Manuf.* **2018**, *1*, 21–26. [[CrossRef](#)]
27. Hong, Z.; Sun, Y.; Ye, P.; Loy, D.A.; Liang, R. Bio-inspired Compact, High-resolution Snapshot Hyperspectral Imaging System with 3D Printed Glass Lightguide Array. *arXiv* **2022**, arXiv:2209.07777. [[CrossRef](#)]
28. Eckel, Z.C.; Zhou, C.; Martin, J.H.; Jacobsen, A.J.; Carter, W.B.; Schaedler, T.A. Additive manufacturing of polymer-derived ceramics. *Science* **2016**, *351*, 58–62. [[CrossRef](#)]
29. Lezal, D.; Pedlikova, J.; Kostka, P.; Bludska, J.; Poulain, M.; Zavadil, J. Heavy metal oxide glasses: Preparation and physical properties. *J. Non-Cryst. Solids* **2001**, *284*, 288–295. [[CrossRef](#)]
30. Hahn, V.; Messer, T.; Bojanowski, N.M.; Curticean, E.R.; Wacker, I.; Schröder, R.R.; Blasco, E.; Wegener, M. Two-step absorption instead of two-photon absorption in 3D nanoprinting. *Nat. Photonics* **2021**, *15*, 932–938. [[CrossRef](#)]
31. Gissibl, T.; Thiele, S.; Herkommer, A.; Giessen, H. Two-photon direct laser writing of ultracompact multi-lens objectives. *Nat. Photonics* **2016**, *10*, 554–560. [[CrossRef](#)]
32. Jiang, S.; Luo, T. Thulium and/or Holmium Doped Germanosilicate Glasses for Two Micron Lasers. U.S. Patent No. 8,467,423, 18 June 2013.
33. Farsari, M.; Chichkov, B.N. Two-photon fabrication. *Nat. Photonics* **2009**, *3*, 450–452. [[CrossRef](#)]
34. Wang, P.; Ng, A.K.L.; Dowler, A.; Eboroff-Heidepriem, H. Development of low-loss lead-germanate glass for mid-infrared fiber optics: II. preform extrusion and fiber fabrication. *J. Am. Ceram. Soc.* **2021**, *104*, 833–850. [[CrossRef](#)]
35. Zhang, Q.; Chen, G.; Zhang, G.; Qiu, J.; Chen, D. Spectroscopic properties of Ho³⁺/Yb³⁺ codoped lanthanum aluminum germanate glasses with efficient energy transfer. *J. Appl. Phys.* **2009**, *106*, 113102. [[CrossRef](#)]
36. Wu, J.; Yao, Z.; Zong, J.; Jiang, S. Highly efficient high-power thulium-doped germanate glass fiber laser. *Opt. Lett.* **2007**, *32*, 638–640. [[CrossRef](#)]

37. Wu, J.; Jiang, S.; Luo, T.; Geng, J.; Peyghambarian, N.; Barnes, N.P. Efficient thulium-doped 2- μm germanate fiber laser. *IEEE Photonics Technol. Lett.* **2006**, *18*, 334–336.
38. Walsh, B.M.; Barnes, N.P.; Reichle, D.J.; Jiang, S. Optical properties of Tm³⁺ ions in alkali germanate glass. *J. Non-Cryst. Solids* **2006**, *352*, 5344–5352. [[CrossRef](#)]
39. Bayya, S.S.; Chin, G.D.; Sanghera, J.S.; Aggarwal, I.D. Germanate glass as a window for high energy laser systems. *Opt. Express* **2006**, *14*, 11687–11693. [[CrossRef](#)]
40. Bayya, S.S.; Sanghera, J.S.; Aggarwal, I.D.; Wojcik, J.A. Infrared transparent germanate glass-ceramics. *J. Am. Ceram. Soc.* **2002**, *85*, 3114–3116. [[CrossRef](#)]
41. Wang, J.; Lincoln, J.; Brocklesby, W.; Deol, R.; Mackechnie, C.; Pearson, A.; Tropper, A.; Hanna, D.; Payne, D. Fabrication and optical properties of lead-germanate glasses and a new class of optical fibers doped with Tm³⁺. *J. Appl. Phys.* **1993**, *73*, 8066–8075. [[CrossRef](#)]
42. Dumbaugh, W.H. Infrared transmitting germanate glasses. In *Emerging Optical Materials*; SPIE: Bellingham, WA, USA, 1982; pp. 80–85.
43. Geng, J.; Wang, Q.; Jiang, S. High-spectral-flatness mid-infrared supercontinuum generated from a Tm-doped fiber amplifier. *Appl. Opt.* **2012**, *51*, 834–840. [[CrossRef](#)]

Disclaimer/Publisher’s Note: The statements, opinions and data contained in all publications are solely those of the individual author(s) and contributor(s) and not of MDPI and/or the editor(s). MDPI and/or the editor(s) disclaim responsibility for any injury to people or property resulting from any ideas, methods, instructions or products referred to in the content.